Journal of the Optical Society of America B
OPTICAL PHYSICS

Control of high-order harmonic generation with chirped inhomogeneous fields

HUA YUAN,[1] FANG LI,[2,*] AND HUA LONG[1,3]

[1]School of Physics and Wuhan National Laboratory for Optoelectronics, Huazhong University of Science and Technology, Wuhan 430074, China
[2]Laboratory of Optical Information Technology, Wuhan Institute of Technology, Wuhan 430205, China
[3]e-mail: longhua@hust.edu.cn
*Corresponding author: lifang_wit@hotmail.com

Received 8 August 2017; revised 25 September 2017; accepted 26 September 2017; posted 28 September 2017 (Doc. ID 304310); published 19 October 2017

We theoretically investigate high-order harmonic generation (HHG) in the chirped inhomogeneous field. The results show that by using a chirped pulse, the HHG in the inhomogeneous field can be efficiently controlled. The harmonic cutoffs can be extended. Supercontinua with photon energies ranging from 201 to 263 eV and isolated attosecond pulses with durations less than 90 as are produced without carrier–envelope phase stabilization. Furthermore, it is shown that our scheme is robust against the variation of the inhomogeneity of the laser field. All our results are well explained by the quantum and classical analysis.

OCIS codes: (190.7110) Ultrafast nonlinear optics; (190.4160) Multiharmonic generation; (190.2620) Harmonic generation and mixing.

https://doi.org/10.1364/JOSAB.34.002390

1. INTRODUCTION

High-order harmonic generation (HHG) is an extremely nonlinear optical phenomenon in the strong-field laser–atom interaction. It has been used to produce coherent extreme ultraviolet (EUV) and soft x-ray sources [1,2] as well as generate attosecond pulses [3]. Attosecond pulses have offered a robust tool for probing and controlling ultrafast electronic dynamics inside atoms [4–6], molecules [7–13], and solids [14,15]. Many techniques have been developed to generate isolated attosecond pulses (IAPs), such as few-cycle laser pulses [16,17], the polarization gating technique [18,19], and two-color or multicolor fields [20–24].

Recently, HHG in the vicinity of nanostructures has attracted much attention. Due to the surface plasmon resonances within metallic nanostructures, the intensity of the incident laser field can be enhanced by several orders of magnitude. The enhanced laser intensity easily exceeds the threshold intensity for HHG in noble gases [25–30]. In the nanogap where HHG takes place, the enhanced field is spatially inhomogeneous. By using such an inhomogeneous field, HHG in nanostructures shows some novel characteristics [31–37], for example, the generation of even order harmonics, the extension of the harmonic cutoff, and the selection of the quantum path. Furthermore, it has been proposed to generate IAPs with inhomogeneous fields [31,32]. However, almost all of the previous works of HHG in inhomogeneous fields are performed with the chirp-free pulse. In fact, the chirped pulse has been demonstrated to be an efficient method to modulate HHG and generate IAPs in homogeneous fields [38].

In this paper, we have extended the chirped pulse to control HHG in the inhomogeneous field. Based on the quantum and classical analysis, we show that the HHG in the inhomogeneous field can be efficiently controlled by using a slightly chirped pulse. The harmonic cutoffs can be extended. The supercontinua from 201 to 263 eV are obtained against the variation of the carrier–envelope phase (CEP). Then IAPs with durations below 90 as can be created for all the values of CEP from 0 to $-\pi$. Moveover, we have also discussed the influence of the inhomogeneity of the laser field on HHG. We show that our scheme still holds against the variation of the inhomogeneity.

2. THEORETICAL MODEL

In our simulations, we assume that the incident laser is linearly polarized along the $\vec{x}$ direction, and then the electron dynamics are mainly confined along the polarization direction. It is reasonable to model the HHG process by solving the time-dependent Schrödinger equation in one spatial dimension (1D-TDSE), which reads (atomic units are used unless stated otherwise)

$$i\frac{\partial\psi(x,t)}{\partial t} = H(x,t)\psi(x,t) = \left[-\frac{1}{2}\frac{\partial^2}{\partial x^2} + V_{\text{atom}}(x) + V_{\text{laser}}(x,t)\right]\psi(x,t). \quad \mathbf{(1)}$$

Here, $V_{\text{atom}}(x) = -\frac{1}{\sqrt{x^2+\alpha}}$ is the soft-core potential. The soft-core parameter α is chosen to be 0.667 to match the ground ionization potential of the neon atom, which is 0.7925 a.u. $V_{\text{laser}}(x,t) = -E(x,t)x$ is the potential due to the laser–electron interaction. The inhomogeneous field is given by

$$E(x,t) = E_t(t)(1+\varepsilon x), \tag{2}$$

where x is the position of the electron ($x = 0$ refers to the position for the parent ion). The parameter ε determines the strength of the spatial inhomogeneity of the laser field. For example, $\varepsilon = 0.006$ means the field intensity varies by 0.6% over 1 a.u. length.

The field $E_t(t)$ is described as

$$E_t(t) = E_0 f(t)\cos[\omega_0 t + \phi_0 + \delta(t)], \tag{3}$$

where E_0, ω_0, and ϕ_0 are the amplitude, angular frequency, and CEP of the laser field, respectively. The pulse envelope is given by $f(t) = \exp[-2\ln(2)t^2/\tau^2]$, where τ is the full width at half-maximum (FWHM) of the electric field. Here, we adopt the temporal phase $\delta(t) = bt^2$ to introduce the linear chirp, where b is the chirp parameter, which is given by

$$b = \frac{2\ln 2}{\tau^2\tau_0}\sqrt{\tau^2 - \tau_0^2}. \tag{4}$$

Here, τ_0 is the Fourier-limited FWHM. In our simulations, by using the linear chirp with the chirp parameter $b = -0.0271\ \text{fs}^{-2}$, the FWHM of a 800 nm laser pulse is increased from the Fourier-limited FWHM τ_0 of 5 to 8 fs.

We use the split-operator method to solve Eq. (1) [39,40]. To avoid the reflections from the spatial boundaries, at each time step the electron wave function is multiplied by a mask function of the form $\cos^{1/8}$. The neon atom is in the initial state (ground state) before we turn on the laser. The ground state is obtained by imaginary time propagation with the soft-core potential. Once the electron wave function $\psi(x,t)$ is obtained, the time-dependent dipole acceleration can be calculated by

$$\begin{aligned} a(t) &= \frac{d^2\langle x\rangle}{dt^2} \\ &= -\langle\psi(x,t)|[H(x,t),[H(x,t),x]]|\psi(x,t)\rangle. \end{aligned} \tag{5}$$

By Fourier transforming the time-dependent dipole acceleration, we can get the harmonic spectrum, which is given by

$$I_q = |a_q|^2 = \left|\frac{1}{T}\int_0^T a(t)\exp^{(-iqwt)}\mathrm{d}t\right|^2, \tag{6}$$

where T is the duration of the laser pulse. The attosecond pulse can be obtained by superposing several orders of harmonics,

$$I(t) = \left|\sum\nolimits_q a_q \exp^{(iqwt)}\right|^2. \tag{7}$$

Here q corresponds to the harmonic order.

3. RESULTS AND DISCUSSION

Figure 1(a) shows the harmonic spectra in the chirp-free inhomogeneous field. Here, an 8 fs, 800 nm field with laser intensity $I_0 = 3.0 \times 10^{14}\ \text{W/cm}^2$ is adopted. The inhomogeneity parameter ε is 0.006. The CEP ϕ_0 of the laser pulse is chosen to be 0 and $-\pi$. As shown in this figure, the cutoff of the harmonic spectrum with $\phi_0 = 0$ is 263 eV and a 108 eV (from 155 to 263 eV) supercontinuum is obtained near the cutoff. While for the case of $\phi_0 = -\pi$, the harmonic cutoff shrinks back to 201 eV and discrete harmonics are generated in the cutoff region. For comparision, we calculate the harmonic spectra in the chirped inhomogeneous field, as shown in Fig. 1(b). Here, the chirp parameter is chosen to be $b = -0.0271\ \text{fs}^{-2}$, and other parameters are the same as in Fig. 1(a). For the case of $\phi_0 = 0$, the harmonic cutoff is 263 eV, which is the same as that in the chirp-free field. However, the bandwidth of the supercontinuum decreases to 62 eV (from 201 to 263 eV). When CEP ϕ_0 changes to $-\pi$, the harmonic cutoff is extended to 269 eV and the discrete harmonics in the cutoff region disappear compared with the chirp-free case. Furthermore, a supercontinuum with a 79 eV (from 190 to 269 eV) bandwidth is obtained.

To clarify the difference of the harmonic spectra between the chirp-free and chirped inhomogeneous fields, we next investigate the classical electron trajectories and the time–frequency distributions of the harmonic spectra. The classical electron trajectories are calculated based on the three-step model [41]. The results in the chirp-free field with ϕ_0 of 0 and $-\pi$ are presented separately in the left and right columns, respectively, of Fig. 2. For the case of $\phi_0 = 0$, the harmonics near the cutoff are dominated by the highest emission peak (labeled as P_1) around 0.25 T_0, as shown in Fig. 2(c). The classical electron trajectories contributing to the peak P_1 are labeled as R_1 in Fig. 2(a). For R_1, the electron is ionized around $-0.5T_0$ and moves toward the positive-x direction. Since the electron is accelerated by the electric field $E(x,t) = E_t(t)(1+\varepsilon x)$ whose effective peak amplitude increases with

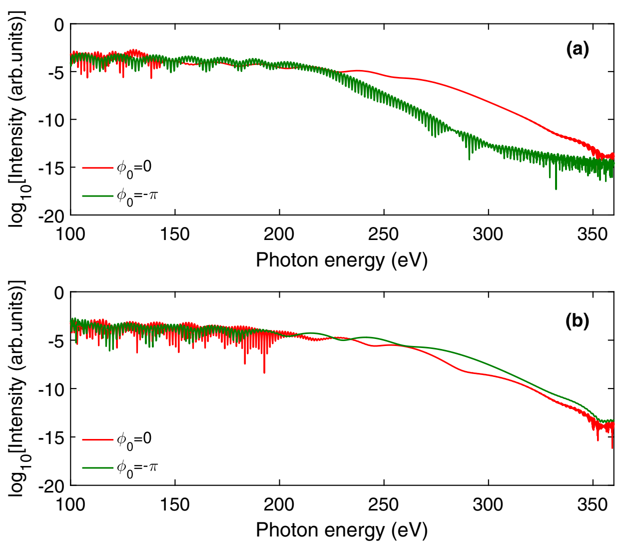

Fig. 1. (a) Harmonic spectra of neon atoms driven by an 8 fs, 800 nm chirp-free inhomogeneous field for two different CEP values of $\phi_0 = 0$ (the red solid line) and $\phi_0 = -\pi$ (the green solid line). (b) Same as (a) but driven by an 8 fs, 800 nm chirped inhomogeneous field with a negative chirp parameter $b = -0.0271\ \text{fs}^{-2}$. In our simulations, except for the chirp parameter, other parameters are the same as in Fig. 1(a).

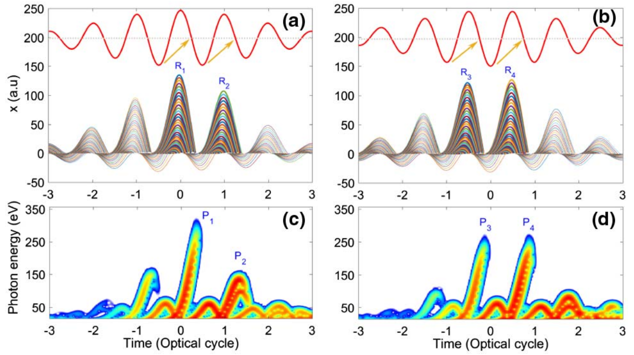

Fig. 2. (a), (c) Classical electron trajectories and time–frequency distribution in the 8 fs, 800 nm chirp-free inhomogeneous field for the case of $\phi_0 = 0$. The electric field is inset in (a) (the red solid line). (b), (d) The same as (a) and (c) but for the case of $\phi_0 = -\pi$. In our simulations, the parameters are the same as in Fig. 1(a).

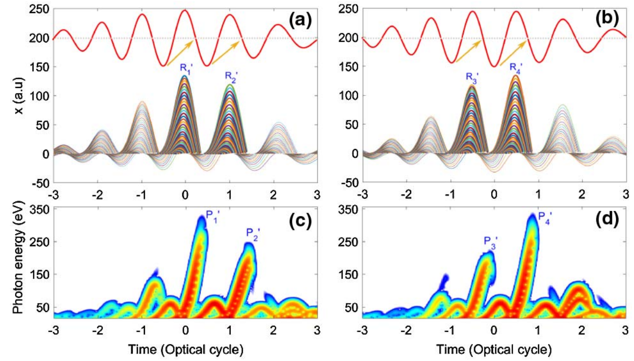

Fig. 3. (a), (c) Classical electron trajectories and time–frequency distribution in the 8 fs, 800 nm chirped inhomogeneous field with a negative chirp parameter $b = -0.0271$ fs^{-2} for the case of $\phi_0 = 0$. The electric field is inset in (a) (the red solid line). (b), (d) The same as (a) and (c) but for the case of $\phi_0 = -\pi$. In our simulations, the parameters are the same as in Fig. 1(b).

$|x|$, the electron gains more energy. The maximum energy of the peak P_1 is 263 eV [Fig. 2(c)], which decides the harmonic cutoff. Besides, for the peak P_1, only the short quantum path survives [32,33]. The maximum energy of the second highest emission peak P_2 is 155 eV. Then a broadband 108 eV (from 155 to 263 eV) supercontinuum is obtained. While in the case of $\phi_0 = -\pi$ in Fig. 2(b), the electron ionized around $-0.5T_0$ moves toward the negative-x direction. The electron is accelerated by the electric field whose effective peak amplitude decreases with $|x|$. The corresponding emission peak around $0.25T_0$ is greatly suppressed [Fig. 2(d)], which only contributes to the low-order harmonics. The harmonics near the cutoff are dominated by the emission peaks P_3 around $-0.25T_0$ and P_4 around $0.75T_0$. The corresponding electron trajectories are labeled as R_3 and R_4, as shown in Fig. 2(b). For R_3 and R_4, the electrons are ionized at about $-T_0$ and 0, respectively, and move toward the positive-x direction. The largest excursion distances of the electrons are close for R_3 and R_4. Then the maximum energies of the peaks P_3 and P_4 are almost the same. The interference of the peaks P_3 and P_4 contributes to the discrete harmonics in the cutoff region [see the green line in Fig. 1(a)]. Moreover, in Fig. 2(b), the electrons of R_3 and R_4 are accelerated by the second strongest peak of the electric field. For the case of $\phi_0 = 0$, the electron of R_1 is accelerated by the strongest one [see Fig. 2(a)]. Therefore, the maximum energy of the corresponding emission peaks P_3 and P_4 are smaller than that of the peak P_1. That is why the harmonic cutoff is suppressed in the case of $\phi_0 = -\pi$ [see Fig. 1(a)].

Figure 3 shows the classical electron trajectories and the time–frequency distributions of the harmonic spectra in the chirped inhomogeneous field for the case of $\phi_0 = 0$ (the left column) and $\phi_0 = -\pi$ (the right column). In the case of $\phi_0 = 0$, the harmonics near the cutoff are dominated by the highest emission peak P_1' around 0.25 T_0 in Fig. 3(c). For P_1', the electron is ionized at about -0.5 T_0 and moves toward the positive-x direction [see R_1' in Fig. 3(a)]. This is similar to the chirp-free case with ϕ_0 of 0. However, different from the chirp-free case, the second highest emission peak P_2' shown in Fig. 3(c) is extended to 201 eV. This is because in the trailing edge of the negatively chirped laser pulse, the effective wavelength is longer than that in the chirp-free case.

The electron corresponding to the peak P_2' is accelerated further away from the parent ion [see R_2' in Fig. 3(a)] and gains more energy. As a consequence, the energy difference between the peaks P_1' and P_2' is smaller and the bandwidth of the supercontinuum with $\phi_0 = 0$ is shortened. In the case of $\phi_0 = -\pi$ [Fig. 3(d)], the emission peak P_4', of which the electron is accelerated in the trailing edge of the laser pulse [see R_4' in Fig. 3(b)], is extended to 269 eV. The emission peak P_3' is suppressed to 190 eV compared to the peak P_3 [see Fig. 2(d)] due to the electron acceleration in the leading edge of the laser pulse [see R_3' in Fig. 3(b)]. Therefore, a 79 eV supercontinuum is obtained in the case of $\phi_0 = -\pi$.

In Fig. 4, we discuss the influence of the inhomogeneity on HHG in the chirped inhomogeneous field. Here, the inhomogeneity parameter ε is chosen to be 0.003, 0.005, and 0.007. Other parameters are the same as in Fig. 1(b). As can be seen from Fig. 4, the cutoff extension and supercontinuum generation are robust against the variation of the inhomogeneity of the laser field. Note that we also investigate HHG in the chirped inhomogeneous field with a positive chirp parameter $b = 0.0271$ fs^{-2}. In this case, the cutoff extension and supercontinuum generation still hold. It should be mentioned that when considering the collective effect of HHG from atoms injected into the gap of the bow-tie array, the supercontinuum near the cutoff is mainly from the contribution of the harmonic emissions driven by the laser field with the largest field inhomogeneity.

In the following, we investigate the CEP dependence of the generated harmonic spectrum with the chirped inhomogeneous field in Fig. 5(b). For comparison, the result with the chirp-free inhomogeneous field is also plotted in Fig. 5(a). In our simulations, the CEP ϕ_0 of the 800 nm pulse changes from 0 to $-\pi$, and the other parameters are the same as in Figs. 1(a) and 1(b), respectively. As shown in Fig. 5(a), the spectral profiles present a clear CEP dependence in the chirp-free case. The harmonic cutoffs decrease from 263 to 201 eV and the generated supercontinua are gradually suppressed when ϕ_0 changes from

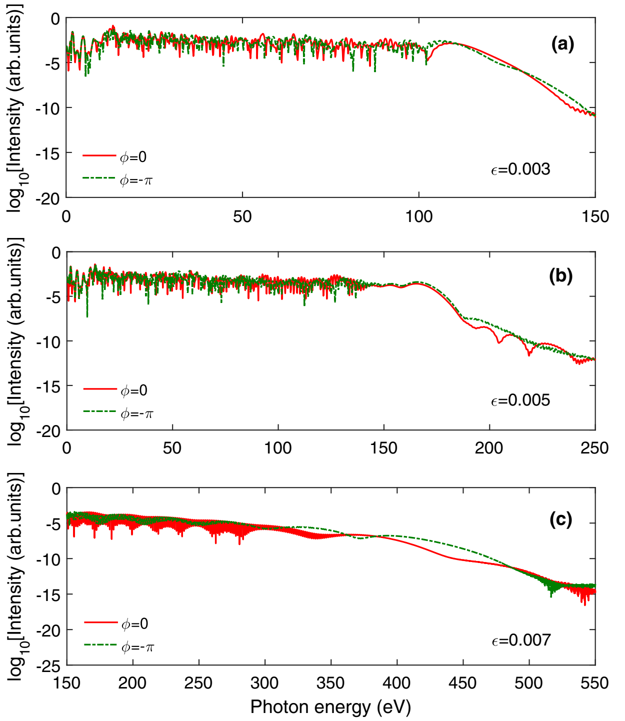

Fig. 4. Harmonic spectra in the chirped inhomogeneous field for the cases $\phi_0 = 0$ (the red solid line) and $\phi_0 = -\pi$ (the green dotted line) with different inhomogeneity parameters: (a) $\varepsilon = 0.003$, (b) $\varepsilon = 0.005$, and (c) $\varepsilon = 0.007$. In our simulations, except for the inhomogeneity parameter, other parameters are the same as in Fig. 1(b).

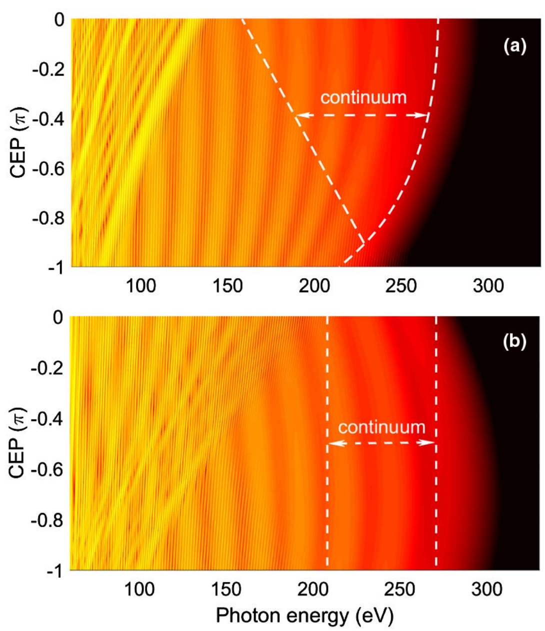

Fig. 5. (a), (b) CEP dependence of the generated harmonic spectrum in the chirped-free and chirped inhomogeneous fields. In our simulations, except for CEP, other parameters are the same as in Figs. 1(a) and 1(b), respectively. The color bar shows the harmonic spectrum in a logarithmic scale.

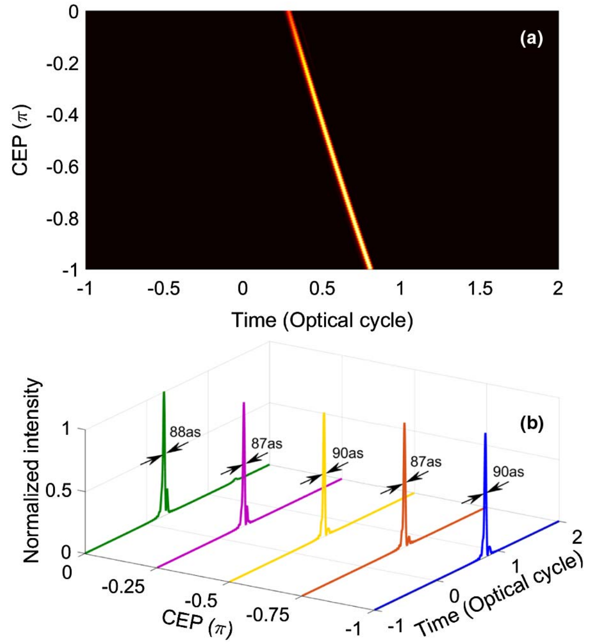

Fig. 6. (a) CEP dependence of IAP generated by synthesizing the harmonics from 201 to 248 eV. (b) Temporal profiles of the IAPs with different CEPs (0, -0.25π, -0.5π, -0.75π, and $-\pi$). In our simulations, except for CEP, other parameters are the same as in Fig. 1(b).

0 to $-\pi$. However, for the case of the chirped field in Fig. 5(b), the harmonic spectra are less sensitive to CEP. The harmonic cutoffs are almost maintained at 263 eV as ϕ_0 varies from 0 to $-\pi$. Supercontinua with photon energies ranging from 201 to 263 eV are obtained against the variation of CEP. It should be stressed that in our simulations, when we use a pulse with a small chirp, a big inhomogeneity parameter should be chosen to keep the CEP independence of the generated harmonic spectrum. On the contrary, for a pulse with a big chirp, the CEP independence of the generated harmonic spectrum can hold with a small inhomogeneity parameter.

Finally, by superposing the broadband supercontinuum from 201 to 248 eV, the CEP-dependent IAP with a chirped inhomogeneous field is presented in Fig. 6(a). One can see that IAPs can be obtained for all the values of CEP from 0 to $-\pi$. For a clear insight, we show the temporal profiles of IAPs with $\phi_0 = 0$, -0.25π, -0.5π, π, and $-\pi$ in Fig. 6(b). It is shown that the durations of IAPs are all below 90 as. It is noted that we also investigate the CEP-dependent IAP in the chirp-free inhomogeneous field by superposing the harmonics from 186 to 232 eV. In this case, IAPs can only be obtained in the range of CEP from 0 to -0.8π. Moreover, due to the gradually suppressed supercontinua, as shown in Fig. 5(a), the durations of IAPs are gradually increased to 130 as when the CEP ϕ_0 changes from 0 to -0.8π.

4. CONCLUSION

In conclusion, HHG in the chirped inhomogeneous field has been investigated. Based on the quantum and classical analysis, we demonstrate that HHG in the inhomogeneous field can be efficiently controlled by using a chirped pulse. The harmonic cutoffs can be extended. As CEP varies from 0 to $-\pi$, the harmonic cutoffs are almost maintained at 263 eV and supercontinua ranging from 201 to 263 eV can be generated. Such supercontinua support the generation of IAPs with durations as short as 90 as. By investigating the influence of the inhomogeneity on HHG, we show our scheme still holds against the variation of the inhomogeneity of the laser field. It is helpful to relax the requirement of CEP stabilization of the laser for the generation of IAPs.

Funding. National Natural Science Foundation of China (NSFC) (11234004, 11404123, 11422435, 11574101, 11627809).

Acknowledgment. Numerical simulations presented in this paper were carried out using the High Performance Computing experimental testbed in SCTS/CGCL.

REFERENCES

1. T. Popmintchev, M. C. Chen, D. Popmintchev, P. Arpin, S. Brown, S. Ališauskas, G. Andriukaitis, T. Balčiunas, O. D. Mücke, A. Pugzlys, A. Baltuška, B. Shim, S. E. Schrauth, A. Gaeta, C. Hernández-García, L. Plaja, A. Becker, A. Jaron-Becker, M. M. Murnane, and H. C. Kapteyn, "Bright coherent ultrahigh harmonics in the keV x-ray regime from mid-infrared femtosecond lasers," Science **336**, 1287–1291 (2012).
2. S. M. Teichmann, F. Silva, S. L. Cousin, M. Hemmer, and J. Biegert, "0.5-keV soft x-ray attosecond continua," Nat. Commun. **7**, 11493 (2016).
3. F. Krausz and M. Ivanov, "Attosecond physics," Rev. Mod. Phys. **81**, 163–234 (2009).
4. M. Uiberacker, T. Uphues, M. Schultze, A. J. Verhoef, V. Yakovlev, M. F. Kling, J. Rauschenberger, N. M. Kabachnik, H. Schröder, M. Lezius, K. L. Kompa, H.-G. Muller, M. J. J. Vrakking, S. Hendel, U. Kleineberg, U. Heinzmann, M. Drescher, and F. Krausz, "Attosecond real-time observation of electron tunnelling in atoms," Nature **446**, 627–632 (2007).
5. E. Goulielmakis, Z. H. Loh, A. Wirth, R. Santra, N. Rohringer, V. S. Yakovlev, S. Zherebtsov, T. Pfeifer, A. M. Azzeer, M. F. Kling, S. R. Leone, and F. Krausz, "Real-time observation of valence electron motion," Nature **466**, 739–743 (2010).
6. Y. Zhou, M. Li, Y. Li, A. Tong, Q. Li, and P. Lu, "Dissection of electron correlation in strong-field sequential double ionization using a classical model," Opt. Express **25**, 8450–8458 (2017).
7. J. Itatani, J. Levesque, D. Zeidler, H. Niikura, H. Pépin, J. C. Kieffer, P. B. Corkum, and D. M. Villeneuve, "Tomographic imaging of molecular orbitals," Nature **432**, 867–871 (2004).
8. C. Zhai, L. He, P. Lan, X. Zhu, Y. Li, F. Wang, W. Shi, Q. Zhang, and P. Lu, "Coulomb-corrected molecular orbital tomography of nitrogen," Sci. Rep. **6**, 23236 (2016).
9. C. Zhai, X. Zhu, P. Lan, F. Wang, L. He, W. Shi, Y. Li, M. Li, Q. Zhang, and P. Lu, "Diffractive molecular-orbital tomography," Phys. Rev. A **95**, 033420 (2017).
10. S. Baker, J. S. Robinson, C. A. Haworth, H. Teng, R. A. Smith, C. C. Chirilă, M. Lein, J. W. G. Tisch, and J. P. Marangos, "Probing proton dynamics in molecules on an attosecond time scale," Science **312**, 424–427 (2006).
11. M. He, Y. Zhou, Y. Li, M. Li, and P. Lu, "Revealing the target structure information encoded in strong-field photoelectron hologram," Opt. Quantum Electron. **49**, 232 (2017).
12. P. Lan, M. Ruhmann, L. He, C. Zhai, F. Wang, X. Zhu, Q. Zhang, Y. Zhou, M. Li, M. Lein, and P. Lu, "Attosecond probing of nuclear dynamics with trajectory-resolved high-harmonic spectroscopy," Phys. Rev. Lett. **119**, 033201 (2017).
13. D. Wang, X. Zhu, X. Liu, L. Li, X. Zhang, P. Lan, and P. Lu, "High harmonic generation from axial chiral molecules," Opt. Express **25**, 23502–23516 (2017).
14. A. L. Cavalieri, N. Müller, T. Uphues, V. S. Yakovlev, A. Baltuška, B. Horvath, B. Schmidt, L. Blümel, R. Holzwarth, S. Hendel, M. Drescher, U. Kleineberg, P. M. Echenique, R. Kienberger, F. Krausz, and U. Heinzmann, "Attosecond spectroscopy in condensed matter," Nature **449**, 1029–1032 (2007).
15. X. Liu, X. Zhu, P. Lan, X. Zhang, D. Wang, Q. Zhang, and P. Lu, "Time-dependent population imaging for high-order-harmonic generation in solids," Phys. Rev. A **95**, 063419 (2017).
16. R. Kienberger, E. Goulielmakis, M. Uiberacker, A. Baltuska, V. Yakovlev, F. Bammer, A. Scrinzi, T. Westerwalbesloh, U. Kleineberg, U. Heinzmann, M. Drescher, and F. Krausz, "Atomic transient recorder," Nature **427**, 817–821 (2004).
17. E. Goulielmakis, M. Schultze, M. Hofstetter, V. S. Yakovlev, J. Gagnon, M. Uiberacker, A. L. Aquila, E. M. Gullikson, D. T. Attwood, R. Kienberger, F. Krausz, and U. Kleineberg, "Single-cycle nonlinear optics," Science **320**, 1614–1617 (2008).
18. Z. Chang, "Chirp of the single attosecond pulse generated by a polarization gating," Phys. Rev. A **71**, 023813 (2005).
19. G. Sansone, E. Benedetti, F. Calegari, C. Vozzi, L. Avaldi, R. Flammini, L. Poletto, P. Villoresi, C. Altucci, R. Velotta, S. Stagira, S. D. Silvestri, and M. Nisoli, "Isolated single-cycle attosecond pulses," Science **314**, 443–446 (2006).
20. T. Pfeifer, L. Gallmann, M. J. Abel, P. M. Nagel, D. M. Neumark, and S. R. Leone, "Heterodyne mixing of laser fields for temporal gating of high-order harmonic generation," Phys. Rev. Lett. **97**, 163901 (2006).
21. P. Lan, E. J. Takahashi, and K. Midorikawa, "Optimization of infrared two-color multicycle field synthesis for intense-isolated-attosecond-pulse generation," Phys. Rev. A **82**, 053413 (2010).
22. S. Haessler, T. Balčiūnas, G. Fan, L. E. Chipperfield, and A. Baltuška, "Enhanced multi-colour gating for the generation of high-power isolated attosecond pulses," Sci. Rep. **5**, 10084 (2015).
23. L. Li, X. Zhu, P. Lan, L. He, and P. Lu, "Photon channel perspective on high harmonic generation," arXiv:1702.04084 [physica.atom-ph].
24. S. A. Rezvani, Z. Hong, X. Pang, S. Wu, Q. Zhang, and P. Lu, "Ultrabroadband tunable OPA design using a spectrally broadened pump sourced," Opt. Lett. **42**, 3367–3370 (2017).
25. S. Kim, J. Jin, Y. J. Kim, I. Y. Park, Y. Kim, and S. W. Kim, "High-harmonic generation by resonant plasmon field enhancement," Nature **453**, 757–760 (2008).
26. M. Sivis, M. Duwe, B. Abel, and C. Ropers, "Nanostructure-enhanced atomic line emission," Nature **485**, E1–E3 (2012).
27. S. Kim, J. Jin, Y. J. Kim, I. Y. Park, Y. Kim, and S. W. Kim, "Kim et al. reply," Nature **485**, E1–E3 (2012).
28. I. Y. Park, S. Kim, J. Choi, D. H. Lee, Y. J. Kim, M. F. Kling, M. L. Stockman, and S. W. Kim, "Plasmonic generation of ultrashort extreme-ultraviolet light pulses," Nat. Photonics **5**, 677–681 (2011).
29. M. Sivis, M. Duwe, B. Abel, and C. Ropers, "Extreme-ultraviolet light generation in plasmonic nanostructures," Nat. Phys. **9**, 304–309 (2013).
30. M. B. Raschke, "High-harmonic generation with plasmonics: feasible or unphysical?" Ann. Phys. **525**, A40–A42 (2013).
31. J. Luo, Y. Li, Z. Wang, Q. Zhang, and P. Lu, "Ultra-short isolated attosecond emission in mid-infrared inhomogeneous fields without CEP stabilization," J. Phys. B **46**, 145602 (2013).
32. I. Yavuz, E. A. Bleda, Z. Altun, and T. Topcu, "Generation of a broadband XUV continuum in high-order-harmonic generation by spatially inhomogeneous fields," Phys. Rev. A **85**, 013416 (2012).
33. M. F. Ciappina, S. S. Aćimović, T. Shaaran, J. Biegert, R. Quidant, and M. Lewenstein, "Enhancement of high harmonic generation by confining electron motion in plasmonic nanostrutures," Opt. Express **20**, 26261–26274 (2012).
34. F. Wang, W. Liu, L. He, L. Li, B. Wang, X. Zhu, P. Lan, and P. Lu, "Macroscopic effect of plasmon-driven high-order-harmonic generation," Phys. Rev. A **96**, 033407 (2017).
35. J. A. Pérez-Hernández, M. F. Ciappina, M. Lewenstein, L. Roso, and A. Zaïr, "Beyond carbon k-edge harmonic emission using a spatial and temporal synthesized laser field," Phys. Rev. Lett. **110**, 053001 (2013).
36. T. Shaaran, M. F. Ciappina, R. Guichard, J. A. Pérez-Hernández, L. Roso, M. Arnold, T. Siegel, A. Zaïr, and M. Lewenstein,

"High-order-harmonic generation by enhanced plasmonic near-fields in metal nanoparticles," Phys. Rev. A **87**, 041402 (2013).
37. L. He, Z. Wang, Y. Li, Q. Zhang, P. Lan, and P. Lu, "Wavelength dependence of high-order-harmonic yield in inhomogeneous fields," Phys. Rev. A **88**, 053404 (2013).
38. J. Xu, B. Zeng, and Y. Yu, "Extension of harmonic cutoff in a multicycle chirped pulse combined with a chirp-free pulse," Phys. Rev. A **82**, 053822 (2010).
39. M. D. Feit, J. A. Fleck, and A. Steiger, "Solution of the Schrödinger equation by a spectral method," J. Comput. Phys. **47**, 412–433 (1982).
40. Z. Wang, M. Li, Y. Zhou, P. Lan, and P. Lu, "Correlated electron-nuclear dynamics in above-threshold multiphoton ionization of asymmetric molecule," Sci. Rep. **7**, 42585 (2017).
41. P. B. Corkum, "Plasma perspective on strong field multiphoton ionization," Phys. Rev. Lett. **71**, 1994–1997 (1993).